



Fermi National Accelerator Laboratory

FERMILAB-Pub-96/113

Accelerator Related Background in the CMS Detector at LHC

A.I. Drozhdin, M. Huhtinen and N.V. Mokhov

*Fermi National Accelerator Laboratory
P.O. Box 500, Batavia, Illinois 60510*

May 1996

Submitted to *Nuclear Instruments and Methods in Physics Research A*

Disclaimer

This report was prepared as an account of work sponsored by an agency of the United States Government. Neither the United States Government nor any agency thereof, nor any of their employees, makes any warranty, expressed or implied, or assumes any legal liability or responsibility for the accuracy, completeness, or usefulness of any information, apparatus, product, or process disclosed, or represents that its use would not infringe privately owned rights. Reference herein to any specific commercial product, process, or service by trade name, trademark, manufacturer, or otherwise, does not necessarily constitute or imply its endorsement, recommendation, or favoring by the United States Government or any agency thereof. The views and opinions of authors expressed herein do not necessarily state or reflect those of the United States Government or any agency thereof.

Accelerator Related Background in the CMS Detector at LHC*

A. I. Drozhdin[†], M. Huhtinen[‡] and N. V. Mokhov

Fermi National Accelerator Laboratory

P.O. Box 500, Batavia, Illinois 60510

[†] *DESY, 22603 Hamburg, Germany*

[‡] *CERN, CH-1211 Geneva, Switzerland*

May 15, 1996

Abstract

Complete calculations of the accelerator related background in the muon spectrometer of the CMS detector at the Large Hadron Collider are presented. The simulations have been performed with the STRUCT multi-turn tracking code and the MARS and FLUKA cascade codes taking into account latest information of the LHC lattice, vacuum conditions, beam cleaning system and the shielding and layout of the CMS experiment. Beam loss distributions in the interaction regions and their vicinities and their contribution to the background levels in the muon spectrometer of CMS are analyzed. The studies show that hadronic and electromagnetic components of machine background are efficiently suppressed by the proposed CMS shielding. High energy muons penetrate through the shielding, but in positions of significance they do not contribute more than a few percent compared to the background generated by the pp -collisions. It is anticipated that the relative contribution of accelerator background will be higher during the first years of operation, but will drop down with the LHC performance evolution. The obtained results concerning the machine background and the efficiency of the proposed shielding are rather generic and can be directly applied to the ATLAS detector.

*Submitted to *Nuclear Instruments and Methods in Physics Research A*

Contents

1	Introduction	3
2	The Large Hadron Collider	4
3	The CMS Experiment	5
4	Beam Losses and Background Origin	6
5	Calculation Sequence	8
6	Production of Particles Entering the CMS Area	12
7	Background in the CMS Muon system	15
8	Comparison of Accelerator and pp Backgrounds in CMS	18
9	Background and LHC Performance Evolution	24
10	Conclusions	24
11	Acknowledgements	25
	References	25

1 Introduction

The overall detector performance at the Large Hadron Collider (LHC) as well as at any other high-luminosity collider, is strongly dependent on the background particle rates in various detector components. Particles originating from the interaction point (IP) and the cascades initiated by them, to be called pp -background in the remainder of this paper, are known to be the major source of background and damage in the detectors at hadron colliders, in the experimental halls and in the final focus triplets. The pp -background in the LHC detectors has been studied in detail and the necessity for a significant amount of shielding has been proven [1, 2, 3, 4, 5]. The problem is not very different from what was expected at the SSC [6] and what is observed at the Tevatron [7].

In the previous studies for LHC detectors only the pp -background was considered and it was assumed that sufficient shielding can be provided so that the machine does not give a substantial contribution. Experience at existing accelerators [8] and studies for the SSC [18, 19] have shown that such additional shielding is indeed needed. The collider detectors are exposed to particle fluxes from the accelerator tunnel. Without dedicated protection, the number of hits from halo particles in the detector can be equal to or even greater than the number of hits originating from the pp -background [8, 9]. Especially dangerous are high energy muons, which are produced mainly in π , K or heavy flavour decays following the interaction of beam particles with machine elements or residual gas in the vacuum pipe.

Studies of muon fluxes entering the experimental areas of LHC have started only recently [10, 11, 12]. One deficiency of the first estimates has been that the beam cleaning system and vacuum conditions of the LHC had not converged to stable design values at the time of the studies. Therefore, e. g., the calculations [11] were based on rather pessimistic assumptions and resulted in unacceptably high background estimates at the experiments. These high values motivated a concentrated effort on the reliable estimation of background emerging from the LHC machine into the experimental areas [13].

In this paper we will concentrate on the CMS area at LHC, although most results and conclusions are rather generic and can be directly applied to the ATLAS detector [2]. We summarize the results of a dedicated simulation study taking into account all beam loss conditions. In addition to muons the fluxes of other particle types emerging from the LHC machine into the experimental region are calculated for the first time. These particles can be classified in four general groups: muons, neutrons, charged hadrons and photons. The muon system of CMS is surrounded by shielding, which efficiently suppresses incident electrons. Thus the photons act as the drivers of the electron flux and the latter can be included as a photon efficiency factor.

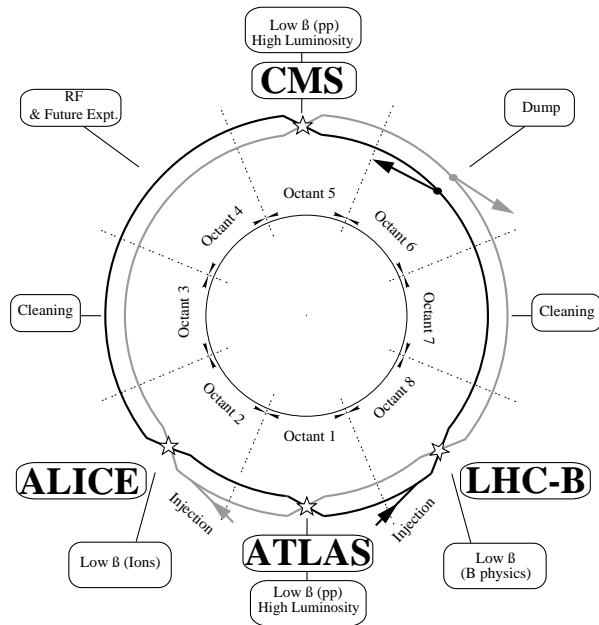


Figure 1: Layout of the LHC machine [14].

2 The Large Hadron Collider

The LHC [14], to be housed in the existing LEP tunnel at CERN, has a circumference of almost 27 kilometres. It will accelerate two countercirculating proton beams up to an energy of 7 TeV. The nominal beam current at the start of a fill is 530 mA. The corresponding nominal luminosity at the two low- β insertions is $10^{34} \text{ s}^{-1} \text{ cm}^{-2}$. Figure 1 shows a schematic layout of the machine, indicating the experimental areas. ATLAS and CMS are the two general purpose high-luminosity pp -experiments. ALICE is a dedicated heavy ion experiment and LHC-B is designed for B-physics studies at reduced luminosity. The LHC will have both momentum and betatron cleaning insertions, which will be either separate as assumed in the present layout, or merged into one single insertion. These cleaning insertions are mandatory, since the maximum beam loss rate into the vacuum chamber, tolerated by the superconducting magnets, is estimated to be 7×10^6 beam protons per meter per second in a limited azimuth range [14]. The injected beams from the SPS accelerator have an initial energy of 450 GeV. The ramp-up takes about 20 minutes. The optimum fill duration, taking into account beam life-time and the time required to refill and accelerate a new beam, is estimated to be about 7 hours in which case the average luminosity would be 60% of the nominal one [14].

Figure 2: Longitudinal view of the CMS detector indicating the location of the different sub-detectors. The tracker is inside the electromagnetic calorimeter (EB and EF).

3 The CMS Experiment

CMS (Compact Muon Solenoid) [1] is one of the two general purpose experiments foreseen for the high-luminosity physics at LHC. A general view of the detector is shown in Figure 2. The main feature of CMS is a large solenoidal magnet, providing a uniform 4 T field over a length of 13 m and a radius of almost 3 m. The flux returns in a massive iron yoke, where four layers of muon stations are embedded. At the center of the experiment is a high-precision central tracker based on silicon pixel, silicon strip and microstrip gas chamber (MSGC) technologies. The tracker is surrounded by an electromagnetic calorimeter (EB and EF). To achieve the best possible energy resolution, a homogeneous crystal solution is adopted. The crystals are PbWO_4 , which allows for a very compact device – crystals of only 23 cm length provide 25 radiation lengths. The coverage reaches up to a pseudorapidity $\eta = 3.0$, corresponding to an angle of 100 mrad with respect to the beam. Following the ECAL comes a copper/scintillator sampling hadronic calorimeter (HB and HF), which has the same η -coverage as the ECAL. Particles in the forward direction are captured by a very forward calorimeter (VF), which is based on quartz-fiber technology with copper or steel as the absorber. The coverage is up to $\eta = 5.0$.

A significant amount of the energy dissipated in the pp -events escapes the CMS detector in the very forward direction and some of this energy would be absorbed in the superconducting coils of the low- β quadrupoles. In order to reduce the power density in the coils below the quench limit, a copper collimator is positioned upstream of the first quadrupole. This collimator is hit by particles carrying on average a total energy of 2.2 TeV per pp -event. This energy leads to the development of intense hadronic cascades in the collimator and its surroundings. Together with punchthrough in the VF and interactions in the beam pipe between the VF and the collimator, these cascades form the source of an intense radiation background in the experimental cavern. The muon station, which is most endangered by the background generated in the collimator region, is the outermost forward station (MF4). The other chambers profit from the shielding provided by the iron yoke. However, the innermost forward chamber (MF1) has to cope with highest rates, which are mainly due to calorimeter punchthrough and interactions created in the beam pipe material under the chamber [3, 4].

Specialized shielding in the whole forward region has to be used to suppress the background to a level where the muon system can operate. This shielding, as described in the FLUKA simulation code, is shown in Figure 3. The main feature of the shielding system is a relatively light mobile part between the VF and the collimator. A massive fixed part surrounds the collimator and low- β region. The inner parts of the shielding are iron. The material of the outer layers is assumed to be borated magnetite concrete, except for the thin part where it is assumed to be borated polyethylene. The shielding configuration used in the simulation has just a sufficient radius to cover the whole cross section of the LHC tunnel.

4 Beam Losses and Background Origin

Accelerator related background in the detectors is induced by beam losses at limiting apertures of the lattice and by beam interactions with the residual gas nuclei inside the vacuum pipe. The expected beam loss rates are listed in Table 1 for all the envisioned loss-inducing processes [14]: inelastic and elastic beam-gas scattering, inelastic, single diffractive and elastic pp collisions, and machine imperfections. Especially dangerous for the experiments are the losses in the corresponding high-luminosity interaction regions (IR), i. e. in the part of a ring between two arcs, consisting of two dispersion suppressors (DS) and a full straight section with a detector at the IP. The reduction of beam loss rates in the IR and introduction of local shielding are the ways to mitigate the background problem. This has been recently demonstrated at Fermilab [8] where the Tevatron related background has been suppressed by a factor of 7 to 10 via installation of a new collimator (beam loss reduction) and of a 1.5 m concrete wall at the hall-tunnel interface (absorption of low-energy particles from the tunnel). With these measures the background fluxes have been brought

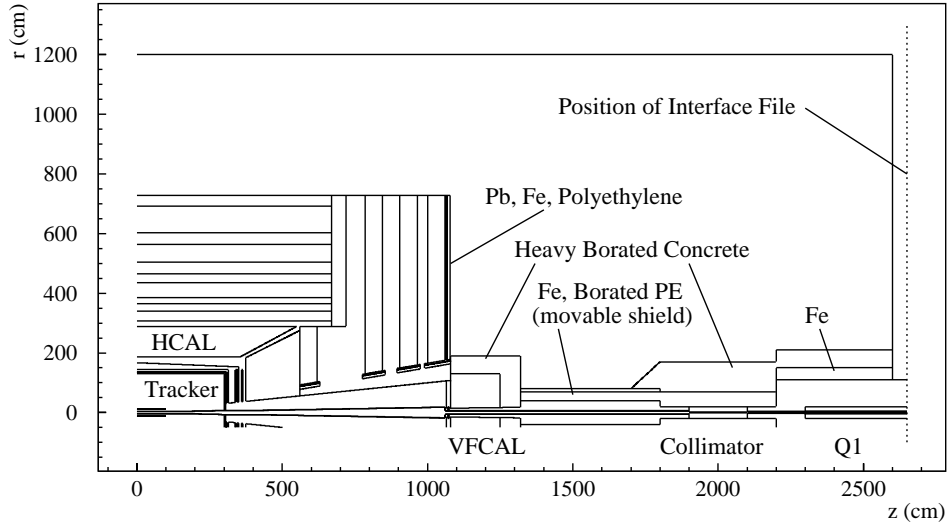


Figure 3: Geometry of the CMS hall as it is used for the FLUKA simulations [4]. Cylindrical symmetry is assumed. The proposed [1, 4] detector-external shielding is indicated.

down to 0.2 Hz/cm^2 (electrons, charged hadrons and muons), 1.2 Hz/cm^2 (photons) and 1.8 Hz/cm^2 (neutrons) at $r=1 \text{ m}$ in the D0 forward muon system. The estimated muon flux reduction alone was about a factor of three.

A highly efficient beam cleaning system is designed for LHC to localize most of the distributed losses (see Table 1) in the two dedicated insertions, IR3 and IR7 [14]. The system, which will be built using room-temperature components, suppresses beam losses in the superconducting magnets to acceptable levels throughout the entire lattice. It was proven [15, 16, 17] that the only scraper system that can handle the multi-TeV proton beam halo at a rate $\geq 10^9 \text{ p/s}$ is one which consists of a set of thin scattering targets followed by secondary collimators. Such a multi-component beam cleaning system has been adopted for the LHC [14] and is used in this study as one of the origins of the residual low-rate beam loss in the IRs. For each beam, a set of three primary collimators and a set of three secondary collimators located in the IR3 (betatron cleaning) are assumed. The thickness of a primary collimator, optimized for 7 TeV, is 0.46 radiation length of carbon, copper or tungsten. Octagonal secondary collimators of 0.5 m thickness are made of copper. The momentum cleaning in the IR7 is presently under study [14], so in this paper it is assumed that the beam cleaning is carried out in the IR3 alone with a total rate of $\approx 3 \times 10^9 \text{ p/s}$ for each beam. It is estimated that 75% of diffractive protons from the pp collisions will end up in the momentum cleaning components in the IR7 and the rest will be lost in the DS. Detailed studies of the resulting beam loss distribution in the LHC lattice are in progress. Table 1 shows an estimation of the beam loss rates and the locations where most of the energy dissipated in the above events will be finally deposited.

Table 1: Beam loss rates from [14] due to different processes for the nominal LHC parameters, two beams and two low- β IRs. The last column shows the expected locations where most of the energy released in the particular process is deposited. Final focus includes low- β quadrupoles, 1.8 m collimators in front of them, D1 separating dipoles and neutral beam dumps (NBD)

Source	Rate (p/s)	Interception location
Beam-gas, <i>in</i>	1.38×10^9	All around the lattice
Beam-gas, <i>el</i>	5.80×10^8	IR3 (betatron cleaning)
<i>pp</i> , <i>in</i>	2.40×10^9	Final focus
<i>pp</i> , <i>sd</i>	4.80×10^8	$\left\{ \begin{array}{l} 25\%: \text{DS in IR} \\ 75\%: \text{IR7 (momentum cleaning)} \end{array} \right.$
<i>pp</i> , <i>el</i>	1.60×10^9	
Imperfections	3.30×10^9	IR3 and IR7 cleaning systems
Cleaning total	5.90×10^9	
Total	9.75×10^9	

With two high-luminosity experiments operating simultaneously diffractive protons from one IP can be lost in the DS elements of another IR and vice versa. The studies [6, 8, 18, 19, 15] and analysis of Table 1 show that with a beam cleaning system embedded into the lattice the beam loss source term in the IP vicinity is composed of the three components:

- beam-gas inelastic interactions in the warm and cold sections of the IR and adjacent arc sections;
- quasi-local interactions of the beam halo tails from the beam cleaning system with the IR components;
- quasi-local interactions of diffractive protons from another IP with the DS components.

Realistic simulations described in the next sections include all three components. Recent studies of the LHC vacuum system [13, 20] give estimates of the average gas densities in IR1, IR2 and IR5. Using these values, we obtain the following beam-gas inelastic interaction rates in the vicinity of IP5:

$$\begin{aligned} &500 \text{ m}^{-1}\text{s}^{-1} \text{ in warm and cold straight sections,} \\ &2 \times 10^4 \text{ m}^{-1}\text{s}^{-1} \text{ in cold arcs.} \end{aligned}$$

5 Calculation Sequence

The calculations are based on the assumption of two high-luminosity experiments operating simultaneously at the nominal luminosity of $10^{34} \text{ cm}^{-2}\text{s}^{-1}$ each. An in-

elastic pp cross section of 80 mb is used, including single diffraction. This corresponds to a slightly higher loss rate than assumed in Table 1 for the pp -collisions. The beam loss calculations of this study are performed only for the clockwise 7 TeV proton beam with 3×10^{14} particles per beam (see Figure 1). The simulations are done in three distinguished stages:

- beam halo particle tracking in the LHC lattice in order to obtain a beam loss distribution in the IR;
- simulation of hadron and electromagnetic cascades induced in the IRs by the above beam losses in order to obtain a sample of particles entering the experimental hall;
- simulation of processes in the detector and experimental area starting with that sample of incident particles.

At the first stage, to simulate the 7×7 TeV pp collisions in IP1 and IP5, the DTUJET93 event generator [21] is used. It is based on the two-component Dual Parton Model which treats both soft (low p_t) and hard (minijet, large p_t) processes in a unified and consistent way. Interactions of 7 TeV protons with nuclei of the residual gas at the rates indicated in the previous section are simulated with the MARS code [22, 23], version 13(96).

Interactions of beam halo with the primary collimators positioned at 6σ from the beam axis, consequent multi-turn particle tracking in the full LHC lattice [14], scoring of particles lost at secondary collimators (7σ from the beam axis) and at all other limiting apertures are performed with the STRUCT code [24], improved over the last couple years. It is assumed that the beam loss rate in the beam cleaning system of IR3 is equally distributed among the three primary collimators, i. e. 10^9 p/s at each of them for each beam. The resulting beam power dissipation in the LHC lattice elements, as obtained from the STRUCT calculations, is shown in Figure 4. The high power peaks correspond to the thin primary collimators. The losses are concentrated in the beam cleaning system at IR3 and – to a much lower level – in the inner triplets of the low- β insertions. The maximum beam loss rate at any single superconducting magnet does not exceed 10^6 p/s per beam for the nominal machine parameters.

At the second stage, shower simulations in the components of the IR and the adjacent arc sections, starting with the beam-gas interactions and the beam loss files obtained by the STRUCT calculations are performed with the MARS code [23]. All the details of the layouts of the high-luminosity insertions at IP1 and IP5, the dispersion suppressors, and the arc half-cells are taken into account at this stage. Three-dimensional geometry and material descriptions of the lattice and tunnel components are taken into account in the simulation model including a 0.4 m horizontal shift of the beam line with respect to the tunnel axis, a floor at 0.95 m beneath the magnet string, a newly proposed flared beam pipe between the D1 dipole and the

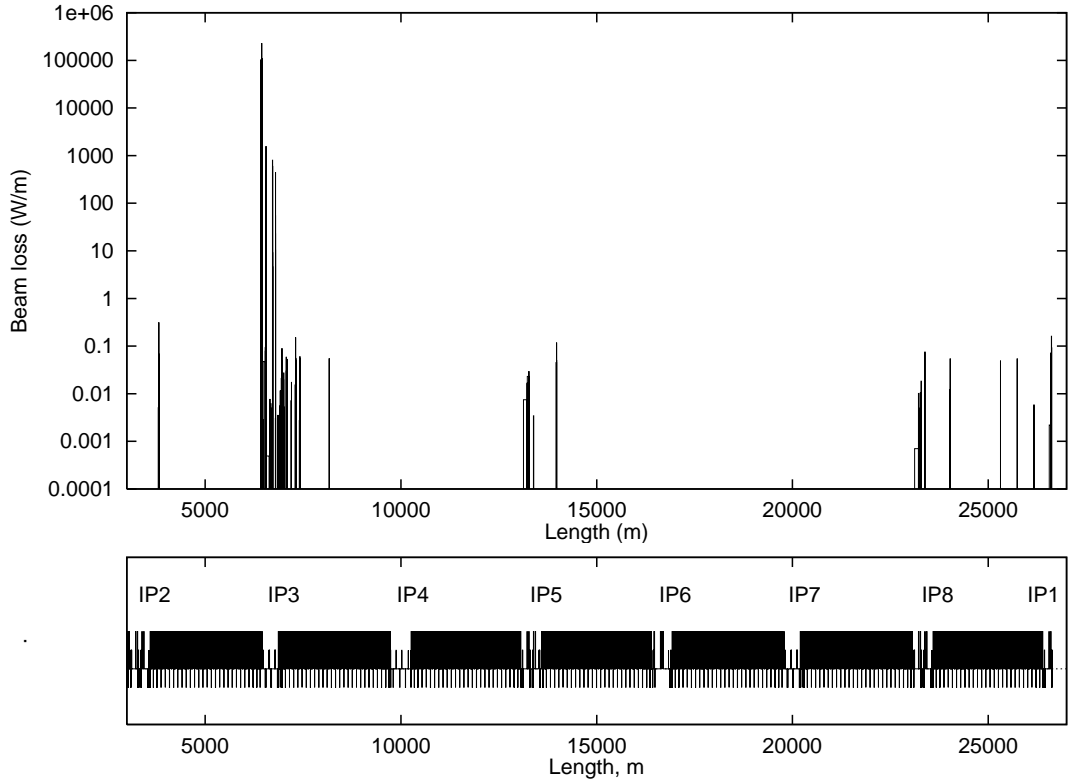


Figure 4: Beam power loss rate in the LHC lattice for the IP3 scrapers as a source. Values are per element divided by the element length.

neutral beam dump (NBD). The twin-aperture NBD itself is assumed to be situated at $z=86.3$ m and to have a length of 3 m. The POISSON calculated 2-D maps of the magnetic field components in the full cross-sections of the low- β quadrupoles, the separation dipoles (D1 and D2), the main dipoles (MB) and main quadrupoles (MQ) are used in the simulations. The shower and muon transport simulations are performed for a clockwise beam in the 1/8 of the LHC lattice adjacent to the IP including the tunnel components and surrounding rock (molasse) with the density of $\rho=2.24$ g/cm³. The rock in the calculations extends 50 m inward, up and down and 1500 m outward of the tunnel.

The version 13(96) of the MARS code used in this study has undergone noticeable improvements since the official release [23]. Related to the considered problem new features include advanced tracking algorithms, an improved hadron-nucleus event generator, prompt muon production by electrons and photons (Bethe-Heitler pairs $\gamma Z \rightarrow Z \mu^+ \mu^-$ and direct positron annihilation $e^+ e^- \rightarrow \mu^+ \mu^-$), muon production in π , K , charmed and vector meson decays and the dimuon continuum, hadron production in photo-nuclear and deep inelastic muon interactions, improved handling of muon transport and of electromagnetic showers associated with a muon track, better geometry handling and histogramming.

This second stage results in files of particles created in the $26.5 \leq z \leq 500$ m region from the IP and entering the experimental hall at $z=26.5$ m and $0 \leq r \leq 10$ m. The coordinate system was selected so that the positive z -axis points against the incoming proton beam. The y -axis is normal to the LHC plane and points upwards and the x -axis points away from the ring center. The cut-off energies for particles in these files are 1 MeV for charged hadrons, muons and e^\pm , 0.2 MeV for photons and 0.5 eV for neutrons.

At the third stage, the particles from the interface files are transported through the experimental area and the CMS detector using the FLUKA95 cascade code [25, 26, 27]. This has the advantage of using exactly the same geometry description and scoring structures as had been previously used for estimating the pp -background [4]. Only a minor modification was made by shifting the shield above the first low- β quadrupole by -0.4 m in the machine plane so that it coincided with the tunnel axis, instead of the beam axis. This shift, which was not included in the previous calculations, should have no significant influence on the pp -background estimates.

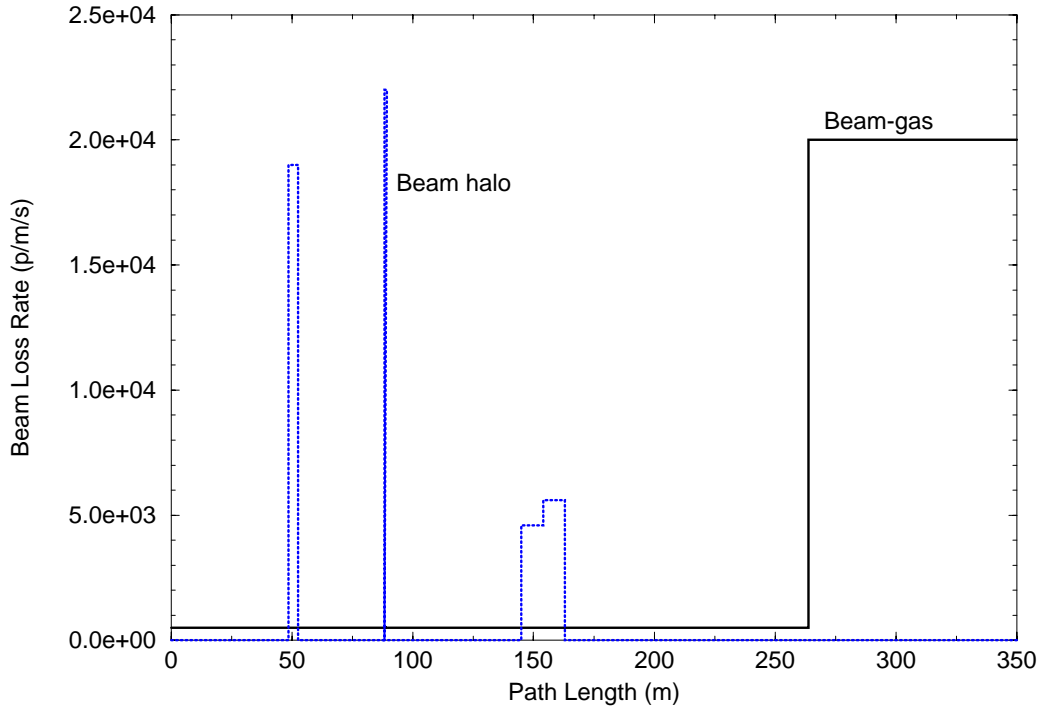


Figure 5: Beam loss rate representation in the IR5.

6 Production of Particles Entering the CMS Area

A simplified representation of the beam loss rate in the IR5 based on the STRUCT calculated file for the beam halo and on the assumed model for the beam-gas rate is shown in Figure 5 as a function of distance from the IP. The plot shows that the potentially dangerous regions are the β_{max} one, the NBD–D2 and D2–Q4 drift spaces, and the cold arc. It is interesting to see how the beam loss distribution structure correlates with the particle fluxes entering the hall. One of the powerful features of the MARS13 code is a tagging technique which allows to mark the source term phase-space regions responsible for a contribution to the calculated values of interest. Figure 6 shows the charged particle flux integrated over the open tunnel cross-section at the hall entrance as a function of the location of the first interaction of a proton with the beam pipe or residual gas nucleus in the 500 m region upstream of the IP. One sees that proton losses in the 200 m long region between Q1 (in the LBQ) and Q5 are responsible for most of the flux entering the experimental hall in the tunnel outside the low- β string.

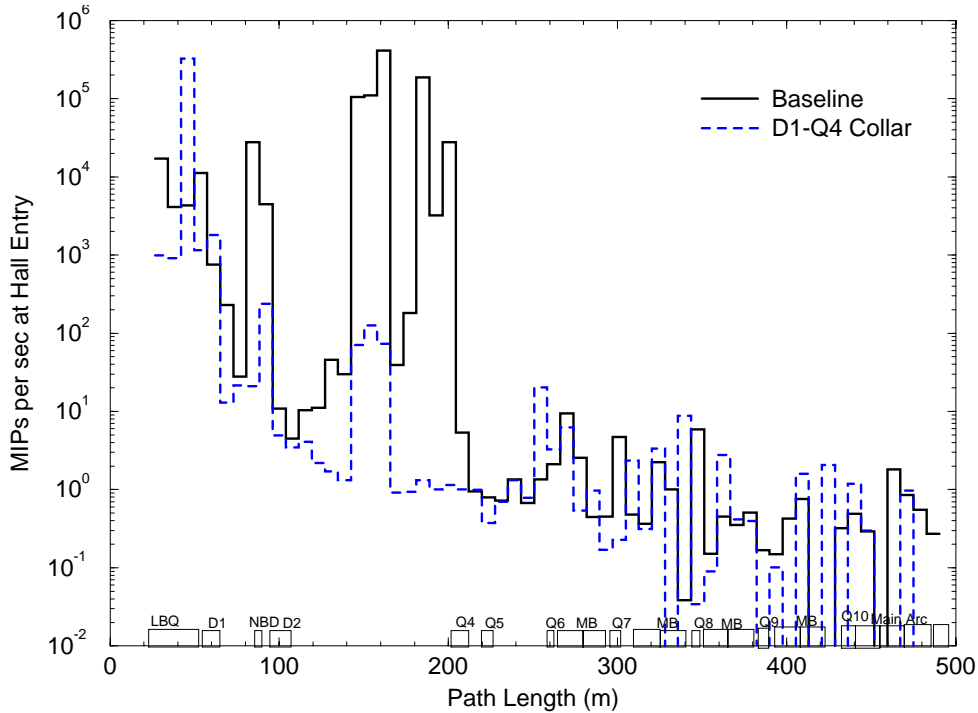


Figure 6: Tagged MIP rate at the hall entry ($z=26.5$ m) in the open tunnel mouth calculated for the baseline case (solid line) and for the case with a steel collar around the beam pipes in the D1–Q4 region (dashed line).

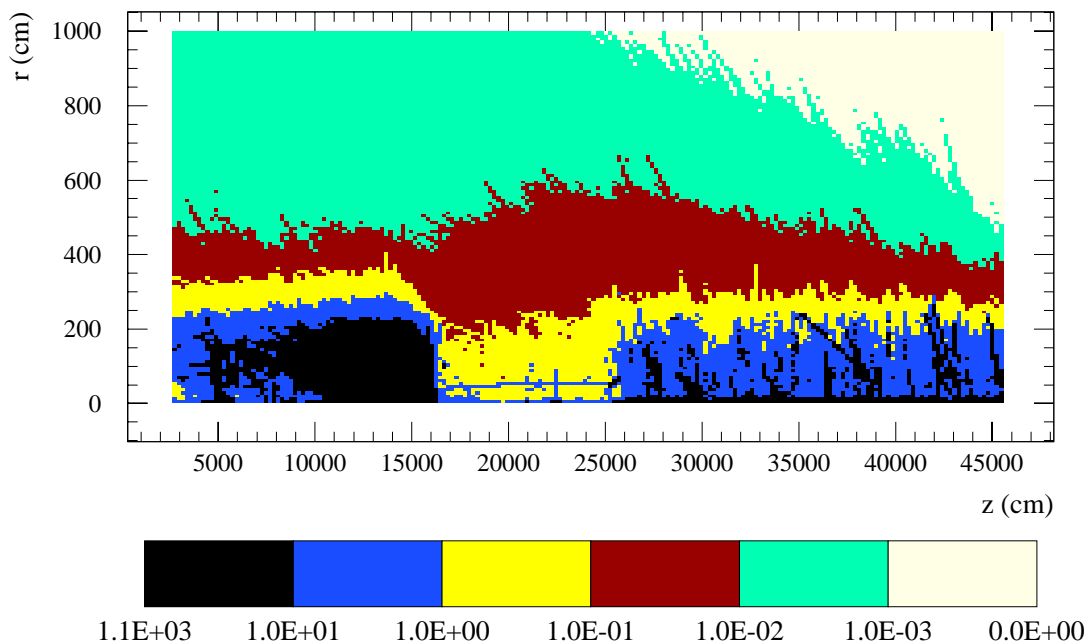


Figure 7: Azimuthally averaged muon isoflux contours ($\text{cm}^{-2}\text{s}^{-1}$) in the IR5 and adjacent arc ($26.5 \leq z \leq 455$ m, $0 \leq r \leq 10$ m).

Muon isoflux contours in the IR5 and adjacent arc components, in the tunnel and the surrounding rock are presented in Figure 7. Beam losses in the entire region up to 500 m from the IP contribute to the muon fluxes entering the detector area. Again, it is clearly seen that the β_{max} region and the open drifts D1 through Q4 are the major source of muons approaching the hall in the tunnel cross-section ($r \leq 1.9$ m).

There are two immediate ways to reduce particle fluxes entering the hall: a shielding plug at the hall-tunnel interface and suppression of muon production. It will be shown that the CMS forward shielding will efficiently plug the tunnel mouth absorbing most of the low energy debris coming to the hall. The muon production and resulting muon rates at the detector can be reduced by suppressing π and K decays in the open drifts. A possible solution would be to surround the bare beam pipes in the D1–NBD, NBD–D2 and, especially, D2–Q4 regions with a steel collar extended up to about a yoke radius. Figure 6 shows the effect of such a collar. It reduces the total charged particle flux at the hall entry ($z=26.5$ m) in the tunnel mouth ($0.43 \text{ m} \leq r \leq 0.95$ m) by a factor of four. The suppression of the total muon flux entering the hall at $r > 1.1$ m (the minimal radius of the MF1 chamber of CMS) is even more remarkable – almost a factor of 17.

The MARS calculations provided the source of particles at the interface to the experimental area. The CMS cavern has slightly curved end walls which in the sim-

ulations have been replaced by a mean half-length of 26 m, so the interface plane was taken to be at $z=26.5$ m from the interaction point. The region between $z=26$ m and $z=26.5$ m was filled with concrete, except for the clearance around the low- β quadrupoles and other beam line elements. This inner radius of the shield was assumed to be 1.10 m. The source was separated into two files, one containing only muons and the other containing all other particles. The normalization of the statistical weights in the interface files was such, that the whole file corresponded to 1 second of LHC operation.

The energy spectra of muons, neutrons, charged hadrons and photons generated in the LHC machine and entering the hall for the high-luminosity experimental areas (CMS or ATLAS) are shown in Figure 8. The most energetic hadrons – including diffractive protons – are all found at small radii, whereas muons of several TeV are detected also outside the magnet string. Table 2 gives the average energies, radii and angles with respect to the beam direction for five particle classes. Although electron flux was not separately scored the electrons are included in the simulation, and give their contribution to the photon flux.

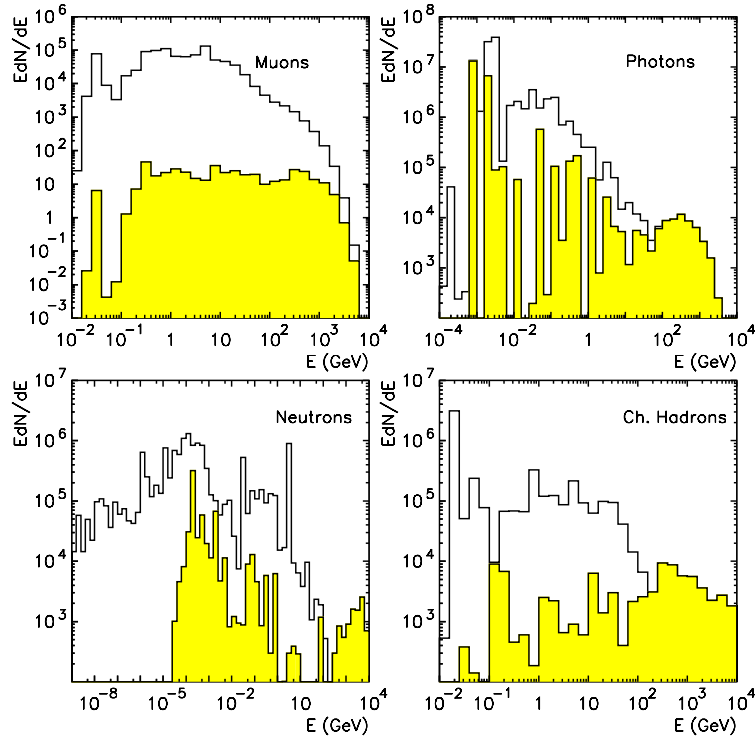


Figure 8: Energy spectra of particles in the MARS-FLUKA interface files at $z=26.5$ m from the LHC interaction point 5. The open histograms show all particles and the shaded ones indicate the contribution by particles for which the radial distance from the beam line is less than 20 cm.

Table 2: Mean energies, radii and angles for different types of particles entering the CMS area. Only particles outside the low- β quadrupoles (i. e. $r > 43$ cm) are considered

Particle	Energy (GeV)	Radius (m)	Angle (rad)
μ	6.59	1.62	0.129
h^\pm	8.11	1.50	0.137
n	0.31	1.33	0.573
e^\pm	0.15	1.38	0.133
γ	0.03	1.76	0.063

7 Background in the CMS Muon system

In the third and final stage of the simulations, the particles from the interface files were transported through the CMS area and detector using the FLUKA95 cascade code [25, 26, 27]. Eight independent runs were performed using the muon file and another eight using the file of other particles. In the muon calculations direct pair production and bremsstrahlung were included explicitly. Muon-hadron interactions were simulated, but the hadron secondaries were not generated. The corresponding energy was deposited at the point of interaction. Shorter test runs were performed with explicit generation of hadron secondaries, to study their contribution and the obtained results for the barrel muon chambers are given in Table 3. A factor of 0.5 was applied to reduce the multiplicity in hadronic interactions. The statistical weight of the surviving particles was correspondingly increased. Leading particle biasing was applied to the electromagnetic interactions, i.e. in each interaction only one of the two secondaries survived – preferentially the more energetic one. The source of particles was assumed to be identical on both sides of the experiment.

Table 3: Particle fluxes ($\text{cm}^{-2}\text{s}^{-1}$) in the barrel muon chambers (MS1–4) of CMS obtained in the actual runs (upper rows) and the shorter runs including explicit generation of hadron secondaries in muon-nuclear interactions (lower rows).

	Neutron	Photon	Muon	Charged Hadron
MS1	$(3.3 \pm 1.2) \times 10^{-3}$	$(8.1 \pm 0.9) \times 10^{-2}$	$(7.2 \pm 0.5) \times 10^{-2}$	$(3.4 \pm 3.4) \times 10^{-6}$
	$(8.2 \pm 3.5) \times 10^{-3}$	$(7.8 \pm 1.4) \times 10^{-2}$	$(5.9 \pm 1.2) \times 10^{-2}$	$(4.4 \pm 2.3) \times 10^{-5}$
MS2	$(2.2 \pm 1.2) \times 10^{-3}$	$(4.1 \pm 0.5) \times 10^{-2}$	$(4.4 \pm 0.4) \times 10^{-2}$	—
	$(1.1 \pm 0.5) \times 10^{-2}$	$(1.2 \pm 0.4) \times 10^{-1}$	$(3.3 \pm 0.1) \times 10^{-2}$	$(9.0 \pm 3.9) \times 10^{-6}$
MS3	$(6.5 \pm 1.2) \times 10^{-3}$	$(9.4 \pm 6.1) \times 10^{-2}$	$(1.5 \pm 0.03) \times 10^{-2}$	$(8.0 \pm 8.0) \times 10^{-8}$
	$(1.0 \pm 0.2) \times 10^{-2}$	$(3.1 \pm 0.8) \times 10^{-2}$	$(1.5 \pm 0.2) \times 10^{-2}$	$(1.2 \pm 0.5) \times 10^{-6}$
MS4	$(3.7 \pm 0.5) \times 10^{-1}$	$(4.0 \pm 0.6) \times 10^{-1}$	$(6.9 \pm 0.5) \times 10^{-3}$	$(4.4 \pm 0.9) \times 10^{-4}$
	$(3.9 \pm 0.9) \times 10^{-1}$	$(3.9 \pm 1.1) \times 10^{-1}$	$(4.5 \pm 0.6) \times 10^{-3}$	$(5.2 \pm 0.9) \times 10^{-4}$

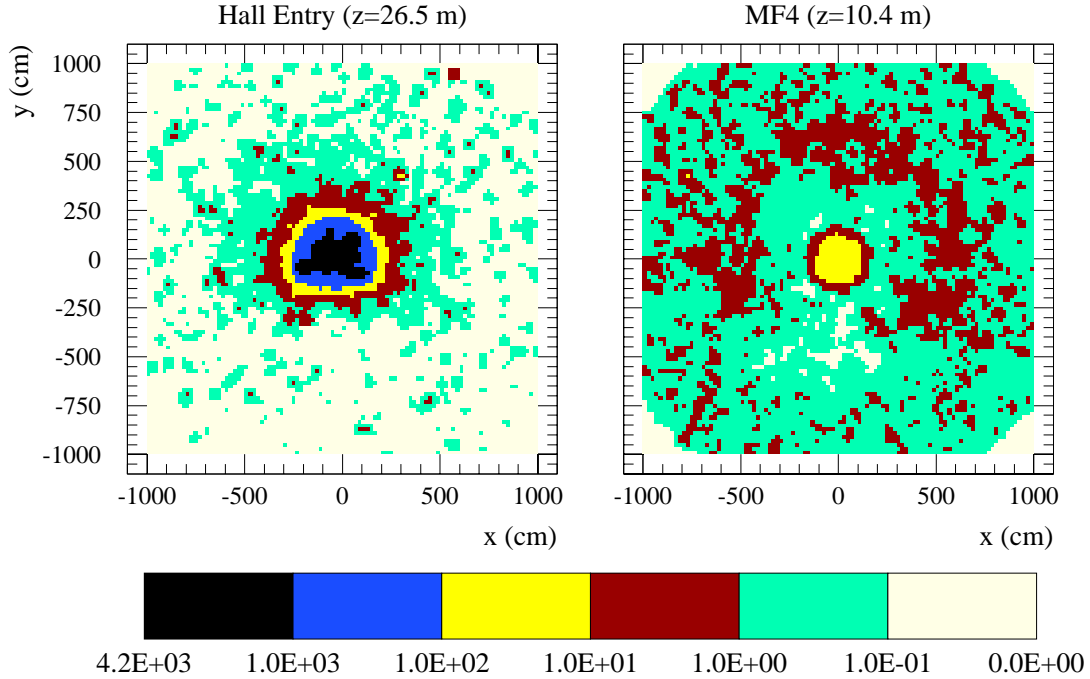


Figure 9: XY-plot of neutron flux ($\text{cm}^{-2}\text{s}^{-1}$) entering the CMS area and in CMS muon station MF4.

The data of the xy-projections suffer from poor statistics. To make the plots more readable, weighted averages over nine bins have been taken, such that the central bin had a weight of 0.4, each of its nearest neighbours 0.09 and each of the diagonal neighbours 0.06. Figure 9 shows an xy-projection of the neutron flux at $z=26.5$ m and in MF4. In the central region the forward shielding of CMS reduces the flux by two orders of magnitude. Most neutrons travel in the air of the tunnel, so that at the $z=26.5$ m plane the shape of the tunnel walls is reflected in the flux. Interactions in the 50 cm concrete layer and the forward shielding completely change the picture and at the MF4 plane the neutrons are almost uniformly distributed, except for the very central part. Since the tunnel is not circular, but has a floor at $y=-95$ cm the forward shielding provides better coverage at $y < 0$. This improved shielding efficiency can be seen as a reduced flux at negative y at the MF4-plane. This effect is even more pronounced in the charged hadron flux, shown in Figure 10. In the charged fluxes the shield essentially removes all particles at radii between 1 and 3 meters. Their remain contributions in the central part are due to punchthrough of high energy hadrons and at large radii due to hadrons passing on top of the shielding.

Longitudinal views of azimuthally averaged neutron and charged hadron flux are shown in Figures 11 and 12, respectively. A comparison clearly illustrates how the charged hadrons act as the driver of the neutron flux. The longitudinal attenuation in the forward shielding is seen to be about 4 orders of magnitude, to be compared with

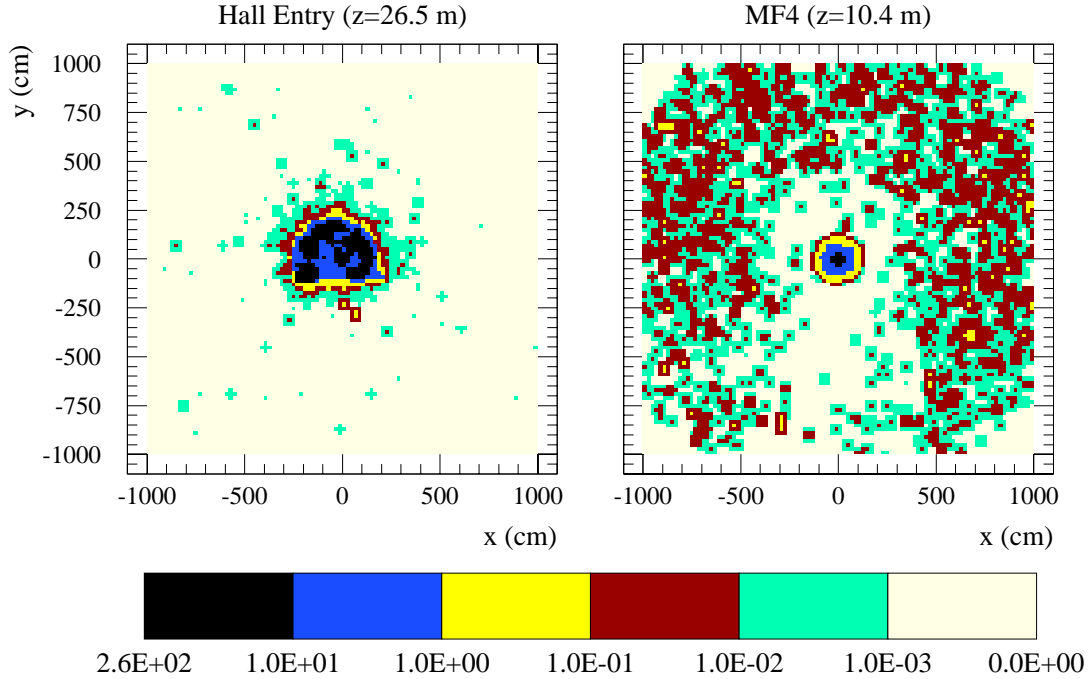


Figure 10: XY-plot of charged hadron flux ($\text{cm}^{-2}\text{s}^{-1}$) entering the CMS area and in CMS muon station MF4.

the 2 orders of magnitude observed in the xy -plots. This difference is explained by the fact that most of the flux leaks through the interface between the tunnel entrance and the forward shielding of CMS. Thus the flux in MF4 does not come through the shield, but around it. In the simulations the overlap between the forward shield and the tunnel entry was only 20 cm, except for the floor region. Most likely the iron and heavy concrete in the last part of the shield will be replaced by conventional concrete, which would increase the shield thickness by 80 cm. The increased overlap should be sufficient to suppress most of the leakage in this region, which would lead to improved shielding with respect to the machine background. The photon flux is qualitatively very similar to the neutron flux shown in Figures 9 and 11.

The xy -projections of the muon flux at the hall entrance and at MF4 are shown in Figure 13. Again the tunnel shape can be recognized, but compared to hadrons the muon flux penetrates more deeply into the rock. Especially the very high energy muons emitted tangentially in the machine plane are clearly visible as a line at $y=0$ extending to positive x . As expected the forward shielding of CMS influences the muon flux much less than the neutron flux. About one order of magnitude attenuation is obtained by the CMS shield.

The corresponding longitudinal-view is shown in Figure 14. The difference to the hadron plots is striking. The longitudinal muon attenuation in the forward shielding amounts only to a factor of about 10, this time in good agreement with the xy -

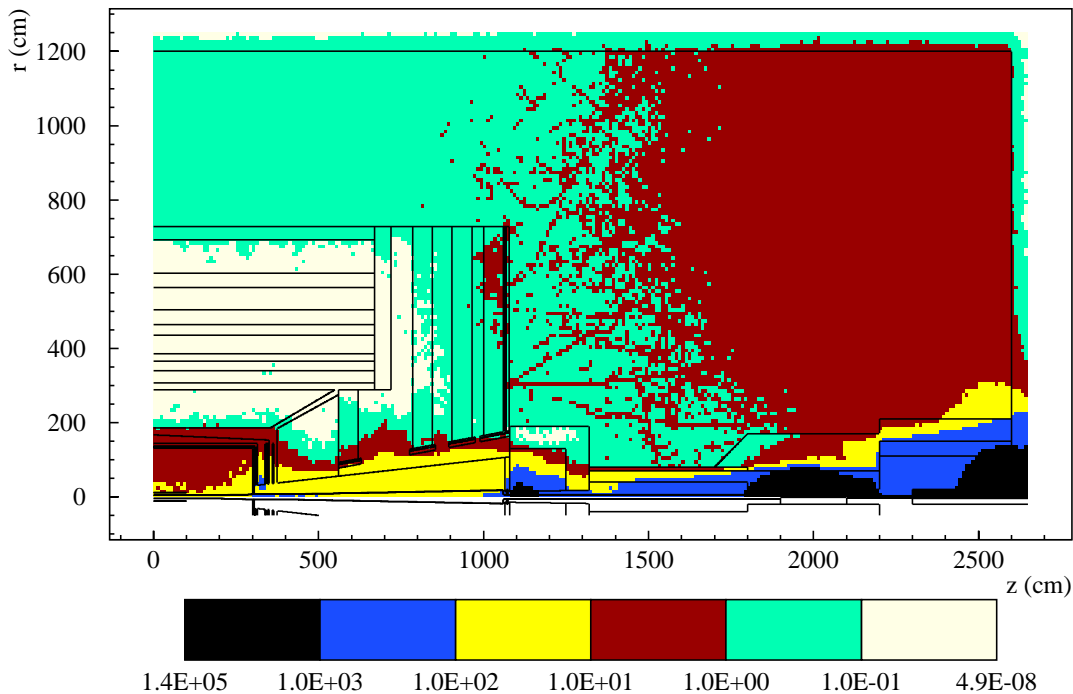


Figure 11: Azimuthally averaged neutron flux ($\text{cm}^{-2}\text{s}^{-1}$) in the CMS experimental area.

plots. This shows that the main contribution of high energy muons comes directly through the shielding and the detector without much disturbance of the muon direction. This leads to bands of equal flux at different radii. Since attenuation along the z -axis is important for these muons, a change of the iron/heavy concrete shield to conventional concrete would slightly increase the number of muons traversing the shield. Only relatively small dilution of the muon flux is observed between $z=26.5$ m and the MF4 plane, so that there is still a recognizable picture of the tunnel shape at MF4. Some low energy muons, associated with interactions in the low-beta region and the shielding, are emitted at large angles to the beam and resemble the flux of charged hadrons, shown in Figure 12. Few tracks in the opposite direction can be also observed. Most of these are due to the equal source on the other side of the detector.

8 Comparison of Accelerator and pp Backgrounds in CMS

Figure 15 shows the machine background and pp -background in the forward muon system of CMS. The latter data is taken from the latest pp -background study which

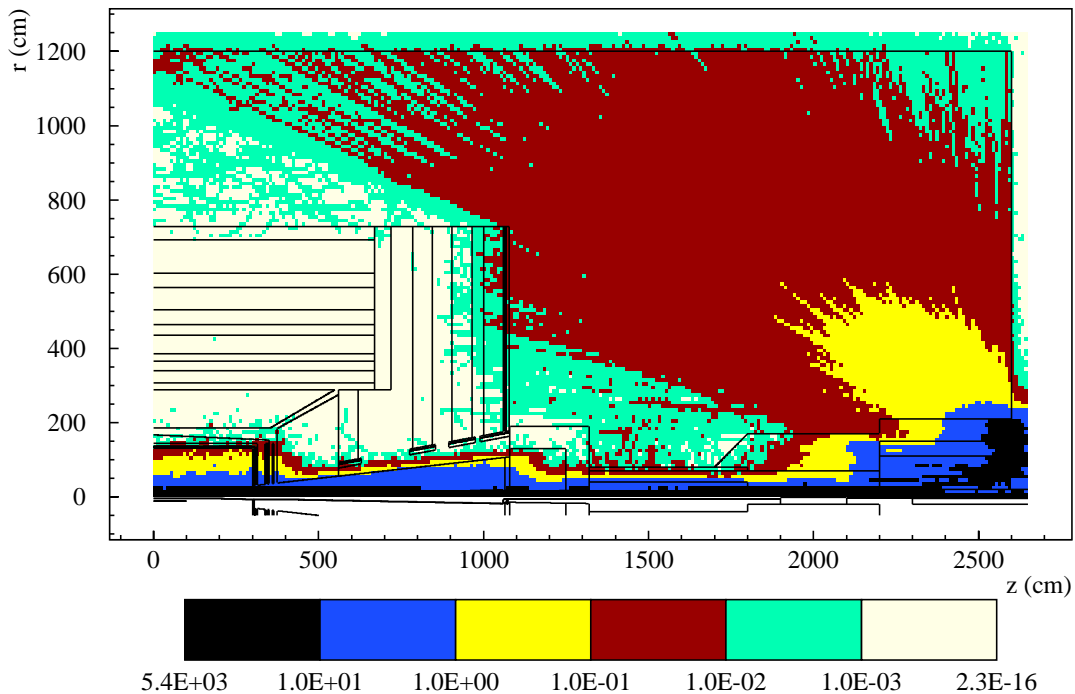


Figure 12: Azimuthally averaged charged hadron flux ($\text{cm}^{-2}\text{s}^{-1}$) in the CMS experimental area.

used the same shielding configuration and simulation methods as now the machine background calculations [4].

The neutron background induced by the machine in the forward muon stations of CMS is 3–5 orders of magnitude lower than the corresponding pp -background at peak luminosity. The direct neutron sensitivity of the muon stations of CMS, however, is very low and photons are always dominating the neutral particle hit rates [3]. The photon flux due to the machine background is 2.5–4 orders of magnitude lower than that created by the pp -background.

As anticipated the most significant background component coming from the machine is formed by muons. Because the option of FLUKA to force meson decays was not used, the simulations in [4] do not provide very good statistics for the muon contribution to the pp -background. The data is, however, sufficient to claim that at large radii and in all of MF3 and MF4 the muon flux originating from the LHC is at least of the same order as the flux originating from the pp -collisions. In addition, these muon hits are associated with a straight high energy track, so their implications for triggers and track reconstruction can be very different from those of randomly distributed hits due to low energy background. The latter usually gives hits only in one or sometimes in a few consecutive Cathode Strip Chambers layers out of the six in a muon station of CMS. This adds to the occupancy, but for a track

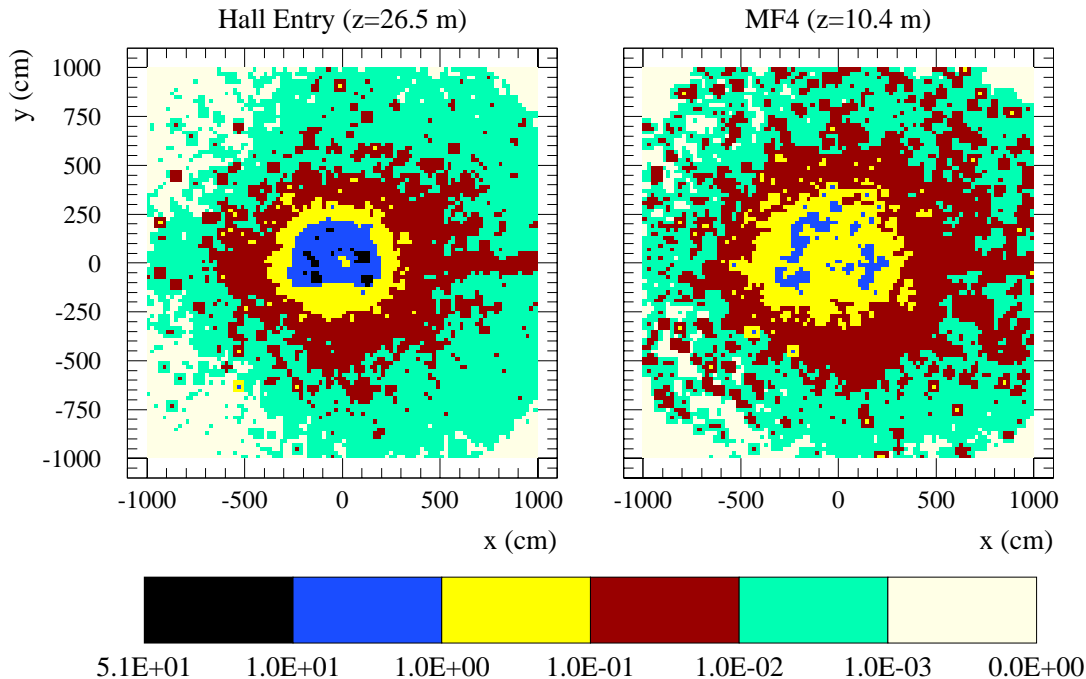


Figure 13: XY-plot of muon flux ($\text{cm}^{-2}\text{s}^{-1}$) entering the CMS area and in CMS muon station MF4.

segment to be accepted correlated hits in at least four out of the six layers are required. Studies for a Resistive Plate Chamber based trigger [28] have shown that such coincidences for random hits are rare, whereas a high energy muon traversing a muon station almost certainly leads to an accepted segment. Another question is if a muon originating from the machine can give a false trigger signal. For this to happen the pattern of several track segments has to point towards the vertex, but within certain tolerances. These tolerances may leave the possibility for obtaining fake triggers from some LHC-muons, but only from a small fraction falling into an unfavourable angular and radial range. Due to this possibility of discarding most of the LHC-muons, the muon rate originating from the pp -interactions will certainly remain dominant, but only detailed trigger simulations will reveal if the difference is one or several orders of magnitude [29]. In all chambers the pp -background flux of charged hadrons is 2–4 orders of magnitude higher than the corresponding flux originating from the machine. Note, however, that the machine induced charged hadron fluxes suffer from poor statistics, especially in MF1 and MF2. Due to the different characteristics of the pp and machine background – especially the contribution by high energy muons – a proper comparison of rates is not straightforward. Figure 16 presents a simplified comparison, by assuming a photon sensitivity of 2% and 100% sensitivity for charged particles. It can be seen that the machine background stays in most parts of the forward muon system at least two orders of magnitude

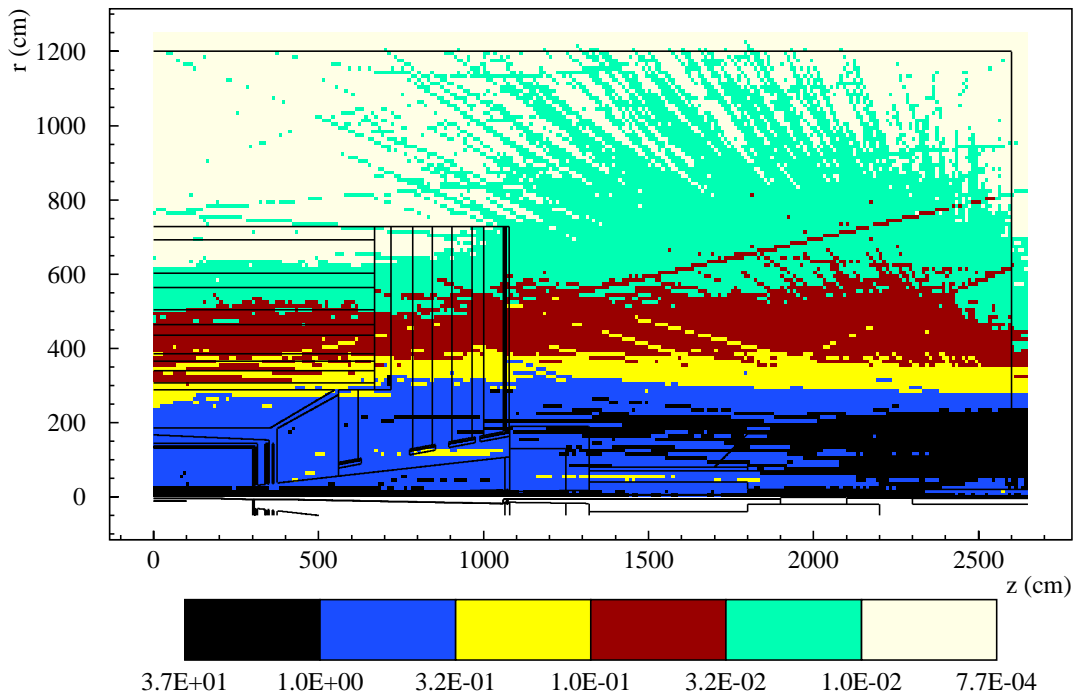


Figure 14: Azimuthally averaged muon flux ($\text{cm}^{-2}\text{s}^{-1}$) in the CMS experimental area.

below the pp -background. Only in the upper parts of MF1, which are shielded by the iron against pp -background from the high- η region, this ratio rises to about 5%. The dotted lines in Figure 16 show the ratio if only the muons from the machine are compared to the total pp -background. A comparison with the solid lines shows, that only at radii larger than 5 m the other particles start to give a contribution, which is of the same order of magnitude as that of the muons. Taking into account that high energy muons and randomly distributed low energy background can have different importances, the effective machine/ pp -background ratio could slightly increase, but certainly not to a level of equal importance.

However, these ratios alone are not quite sufficient to determine the importance of the machine background. It also depends what the total rate is. The highest total rates – reaching up to $500 \text{ cm}^{-2}\text{s}^{-1}$ – are found in MF1 at high η (small radius). Just in this position the machine background is up to three orders of magnitude below the pp -background and thus gives only a negligible contribution. The muon flux from the machine is essentially independent of the longitudinal (z) coordinate. Thus, in regions which are well shielded against the pp -background the machine background is relatively more important. Such regions are the upper parts of MF1 and most of MF2 and MF3. Here the pp -background adds up to a signal rate of $0.5\text{--}100 \text{ cm}^{-2}\text{s}^{-1}$ depending on radius. With an appropriate forward shielding plugging the tunnel

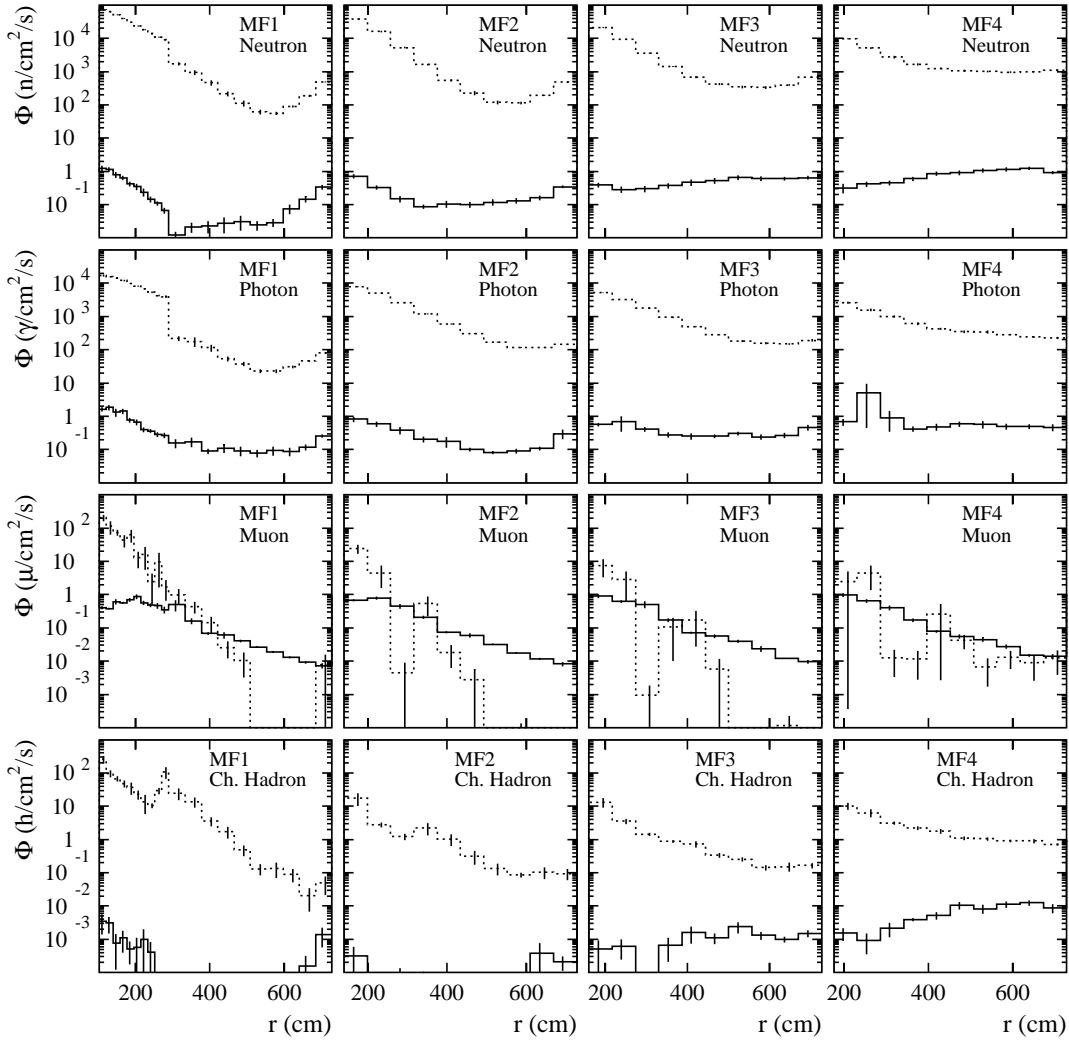


Figure 15: Fluxes of neutrons, photons, muons and charged hadrons in the forward muon system of CMS. The dotted lines show the fluxes due to pp -background and the solid ones the fluxes due to machine background. The bars indicate the 1σ statistical errors of the simulations.

mouth, the machine background is almost entirely due to muons, which give rates from $0.01\text{--}1\text{ cm}^{-2}\text{s}^{-1}$ with a similar radial dependence as the pp -background. In conclusion the machine background in the most exposed regions of the CMS muon system stays at least two orders of magnitude below the pp -background, but can reach almost 10% in regions where the total background is lowest.

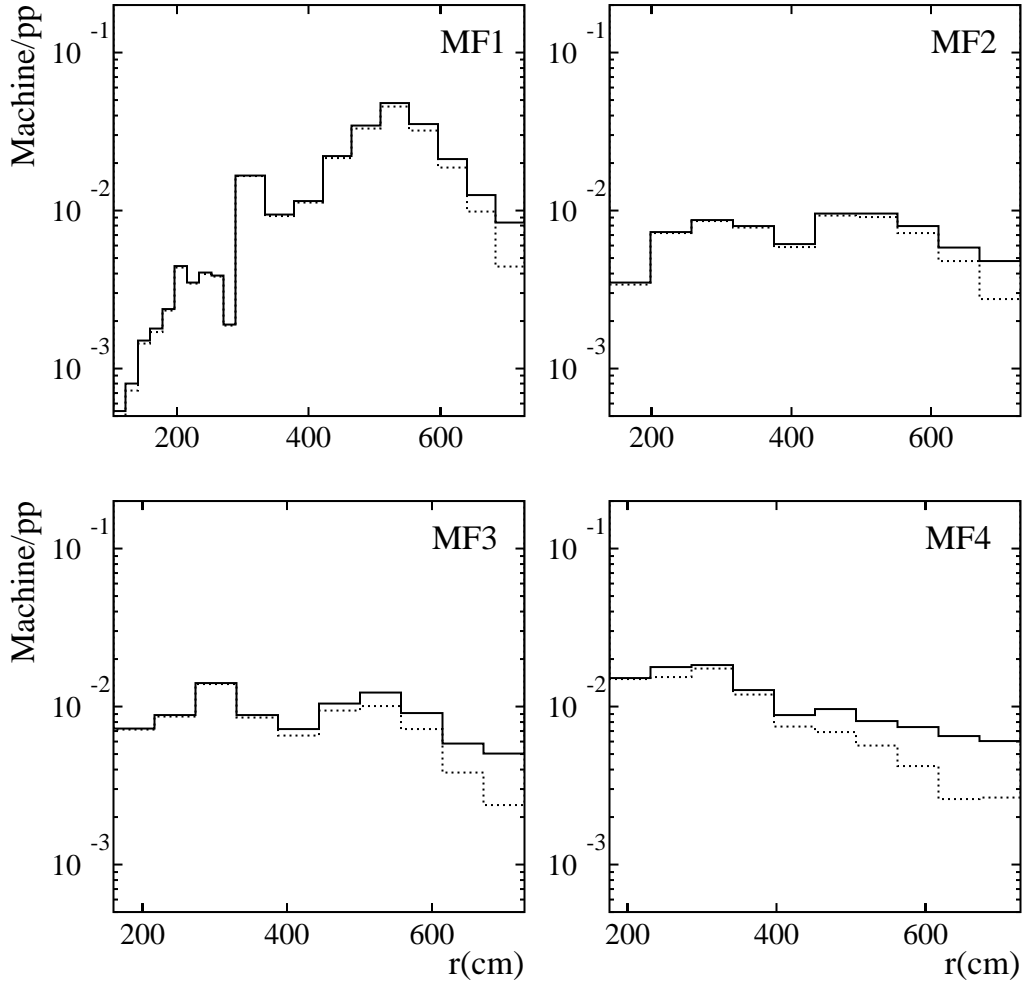


Figure 16: Ratio of background in the forward muon system of CMS due to beam losses in the machine and pp -collisions. The solid line shows a comparison of total background assuming a sensitivity of 2% for photons and 100% for charged particles. The dotted line compares only muons from the machine to the total pp -background.

In the barrel chambers MS2 and MS3, which are completely surrounded by the iron yoke, the pp -background is strongly suppressed. The high energy muons from the machine can penetrate to these chambers. According to Table 3 the longitudinally averaged muon fluxes observed in MS2 and MS3 are $0.05 \text{ cm}^{-2}\text{s}^{-1}$ to $0.02 \text{ cm}^{-2}\text{s}^{-1}$, respectively. The charged hadron background, even if explicit hadron generation is included, is negligible. The corresponding flux estimates for the pp -background add up to values of $0.5 \text{ cm}^{-2}\text{s}^{-1}$ in MS2 and $0.1 \text{ cm}^{-2}\text{s}^{-1}$ in MS3. Thus the ratio between pp -background and machine background in the barrel chambers is about one order of magnitude, in good agreement with the observation for upper

parts of MF1. Again it must be remembered, that this relatively high contribution from the machine is entirely due to the fact that the chambers are so well shielded that the total hit rate is very low.

9 Background and LHC Performance Evolution

All of the preceding discussion concerns LHC operation at nominal parameters and with a perfectly tuned lattice. Several years of initial low luminosity running will be required before LHC reaches these conditions. It is assumed that within its first year of operation LHC would reach one tenth of its design luminosity. It is estimated that the quadratical dependence between beam current and luminosity could be compensated by reducing the emittance so that 10% of nominal luminosity would be achieved with 16% of the nominal beam current. Since machine background depends on the beam current but the pp -background on the luminosity the relative importance of machine background during the low-luminosity phase will be higher by a factor of 1.6. But here again the total background rate will also be lower – corresponding to the reduced performance.

More important than the intensity/luminosity dependence will be the tuning of the machine. Most likely LHC, in its first years, will not be the almost perfectly clean machine it is designed to be. During that period beam losses due to machine imperfections could lead to a significant increase of the relative importance of machine background. However, a hard limit to beam losses is posed by the energy deposition in the superconductors. To stay within the design criteria at 16% of the nominal beam current, the loss rate – relative to the beam current – cannot increase by more than a factor of 6 compared to the nominal values. And consequently, when the beam current and luminosity gradually increase, the relative importance of the beam losses has to decrease approaching finally the values presented in this paper.

10 Conclusions

The muon, neutron, photon and charged hadron background in the CMS detector due to beam losses in the LHC machine has been calculated. To obtain a realistic description of beam losses latest information of the machine lattice and of the vacuum conditions were used. Multi-turn particle tracking with the STRUCT code was coupled to simulation of interactions and cascade development with the MARS code. These two codes were used to obtain a sample of particles entering the CMS experimental area. The final simulation of cascade development in the CMS detector and the associated shielding was performed with the FLUKA cascade code using the latest available description of shield configurations in the CMS area. The emphasis was put on particle fluxes in the muon system of CMS.

The results were compared with previously calculated background due to pp -interactions alone [1, 3, 4]. Hadronic and electromagnetic background is efficiently suppressed by sealing the tunnel entry with a concrete plug. The results of the present studies show, that an overlap of few tens of centimetre between the collimator shielding in the experimental area and tunnel entry is sufficient to almost completely suppress the hadron and photon fluxes emerging from the machine. A recently proposed change of the CMS shielding from magnetite to conventional concrete would increase this overlap from the now assumed 20 cm to about 1 metre and lead to even lower hadron and photon fluxes.

The most important machine background component is due to high energy muons, which are not stopped in the shielding. The muon flux is essentially independent of the longitudinal (z) coordinate, but decreases with increasing radius having, however, a maximum at a radius of about 1.5 m. Therefore the machine muons are relatively most important in the innermost barrel chambers, which are protected by the iron yoke against the less energetic pp -background. Here the machine background can amount to 10% of the total hit rate, but this is only because the total hit rate is insignificant.

In the most exposed areas of the forward muon system, the contribution from the machine stays about two orders of magnitude below the pp -background rate when LHC operates at its nominal parameters. Even when taking into account the different characteristics of the high energy muon tracks and random hits, the pp -background remains still at least a factor of ten more important in the regions where hit rates could become a problem for the chamber performance.

During the first years, when LHC operates at 10% of the nominal luminosity, the relative importance of machine background can be higher. But since the loss rate in the machine cannot exceed the quench limit of the magnets, this increase probably will not exceed a factor of 10.

11 Acknowledgements

We express our gratitude to K. Potter and G. Wrochna for stimulating discussions and to R. Ostojic for providing us with the POISSON calculated magnetic field maps for the LHC quadrupole and dipole magnets.

References

- [1] ‘CMS Technical Proposal’, CERN/LHCC 94-38 (1994).
- [2] ‘ATLAS Technical Proposal’, CERN/LHCC 94-43 (1994).

- [3] M. Huhtinen and P. Aarnio, ‘Neutron and Photon Fluxes and Shielding Alternatives for the CMS Detector at LHC’, Nucl. Instr. and Meth., **A363** (1995) 545.
- [4] M. Huhtinen, ‘Radiation Environment Simulations for the CMS Detector’, in *Proc. of the 2nd Workshop on Simulating Accelerator Radiation Environments*, CERN 9–11th Oct. 1995, CERN CMS TN/95-198 (1995).
- [5] A. Ferrari, K. Potter, S. Rollet and P. R. Sala, ‘Radiation Calculations for the ATLAS Detector and Experimental Hall’, in *Proc. of the 2nd Workshop on Simulating Accelerator Radiation Environments*, CERN 9–11th Oct. 1995, CERN/EST-LEA/01/96 (1996).
- [6] M. Diwan, Y. Fisyak, N. Mokhov et al., ‘Radiation Environment and Shielding for the GEM Experiment at the SSC’, SSCL–SR–1223 (1993).
- [7] N. V. Mokhov, ‘Optimization of the Radiation Environment at the Tevatron’, in *Proc. of the 2nd Workshop on Simulating Accelerator Radiation Environments (SARE2)*, CERN 9–11th Oct. 1995.
- [8] J. Butler, D. Denisov, T. Diehl, A. Drozhdin, N. Mokhov, and D. Wood, ‘Reduction of Tevatron and Main Ring Induced Backgrounds in the D0 Detector’, Fermilab–FN–629 (1995).
- [9] N. V. Mokhov, ‘Comparison of Backgrounds in Detectors for LHC, NLC and $\mu^+ \mu^-$ Colliders’, Fermilab-Conf-96/062 (1996).
- [10] N. Mokhov, ‘Accelerator Related Muon Backgrounds’, in Proc. of the CMS ENDCAP Muon Meeting, U. of Maryland, April 1995.
- [11] I. Azhgirey, V. Talanov, and A. Uzunian, ‘Preliminary Estimations of Muon Fluences on CMS Muon Chambers due to Proton Losses on the LHC Straight Section 5’, CERN CMS TN/95-053 (1995).
- [12] I. Azhgirey, V. Talanov, and A. Uzunian, ‘Background Muons Generated in the CMS Detector Area by the Beam Losses in the LHC’, CERN CMS TN/95-202 (1995).
- [13] Proc. of the Workshop on LHC Backgrounds, CERN, 22 March 1996.
- [14] The LHC Study Group, ‘The Large Hadron Collider, Conceptual Design’, CERN/AC/95-05 (LHC), Ed. P. Lefèvre and T. Pettersson, (1995).
- [15] L. Burnod and J. B. Jeanneret, ‘Beam Losses and Collimation in the LHC: A Quantative Approach’, CERN SL/91–39 (EA), LHC Note 167 (1991).

- [16] M. Maslov, N. Mokhov, and I. Yazynin, ‘The SSC Beam Scraper System’, SSCL–484 (1991).
- [17] A. Drozhdin, N. Mokhov, R. Soundranayagam, J. Tompkins, ‘Toward Design of the Collider Beam Collimation System’, SSCL–Preprint–555 (1994).
- [18] N. V. Mokhov, ‘Accelerator/Experiment Interface at SSC’, in Proc. of the Workshop on Simulating Accelerator Radiation Environments, Santa Fe, January 1993, pp. 12–26, LA–12835–C, UC–414 (1994).
- [19] N. V. Mokhov, ‘Accelerator/Experiment Interface at Hadron Colliders: Energy Deposition in the IR Components and Machine Related Background to Detectors’, Fermilab–Pub–94/085 (1994).
- [20] A. G. Mathewson, *et al.*, CERN LHC Project Notes 19, 20, 27 (1995).
- [21] P. Aurenche, *et al.*, ‘DTUJET-93’, Computer Physics Commun., **83** (1994) 107.
- [22] A. N. Kalinovskii, N. V. Mokhov, and Yu. P. Nikitin, ‘Passage of High-Energy Particles through Matter’, AIP, NY (1989).
- [23] N. V. Mokhov, ‘The MARS Code System User’s Guide, Version 13(95)’, Fermilab–FN–628 (1995).
- [24] I. Baishev, A. Drozhdin, and N. Mokhov, ‘STRUCT Program User’s Reference Manual’, SSCL–MAN–0034 (1994).
- [25] A. Fassò, A. Ferrari, J. Ranft and P. Sala, ‘FLUKA: Present Status and Future Developments’, *Proc of the IV Int. Conf. on Calorimetry in High Energy Physics, La Biodola*, 20–25th Sep. 1993. Ed. A. Menzione and A. Scribano, World Scientific, p. 493 (1993).
- [26] A. Fassò, A. Ferrari, J. Ranft and P. Sala, ‘FLUKA: Performances and Applications in the Intermediate Energy Range’, *Proc of the Specialists’ Meeting on Shielding Aspects of Accelerators, Targets and Irradiation Facilities*. Arlington, Texas, 28–29th Apr. 1994 NEA/OECD doc. p. 287 (1995).
- [27] P. Aarnio, *et al.*, ‘Electron-photon Transport: Always so Good as We Think? Experience with FLUKA’, in *Proc. of MC93, Int. Conf. on Monte Carlo Simulation in High Energy and Nuclear Physics*, p. 100, ed. P. Dragowitsch, S. Linn and M. Burbank, World Scientific (1994).
- [28] M. Huhtinen and G. Wrochna, ‘Estimation of the RPC Muon Trigger Rates Due to Neutral Particles’, CERN CMS TN/94-138 (1994).
- [29] G. Wrochna, private communication.